

RSC Advances



This is an *Accepted Manuscript*, which has been through the Royal Society of Chemistry peer review process and has been accepted for publication.

Accepted Manuscripts are published online shortly after acceptance, before technical editing, formatting and proof reading. Using this free service, authors can make their results available to the community, in citable form, before we publish the edited article. This *Accepted Manuscript* will be replaced by the edited, formatted and paginated article as soon as this is available.

You can find more information about *Accepted Manuscripts* in the [Information for Authors](#).

Please note that technical editing may introduce minor changes to the text and/or graphics, which may alter content. The journal's standard [Terms & Conditions](#) and the [Ethical guidelines](#) still apply. In no event shall the Royal Society of Chemistry be held responsible for any errors or omissions in this *Accepted Manuscript* or any consequences arising from the use of any information it contains.

Fabrication and properties of lightweight ZrB₂ and SiC-modified carbon bonded carbon fiber composites via polymeric precursor infiltration and pyrolysis

Baosheng Xu, Shanbao Zhou, Changqing Hong^{*}, Xinghong Zhang, Jiecai Han

Science and Technology on Advanced Composites in Special Environment Laboratory,
Harbin Institute of Technology, Harbin 150001, PR China

ABSTRACT

To improve the oxidation-resistance of carbon bonded carbon fiber composites (CBCFs), the low density and porous CBCFs modified with ZrB₂ and SiC ceramics with density of 0.26, 0.40, 0.61 and 0.77g/cm⁻³ were prepared by precursor infiltration and pyrolysis method. The pyrolysis behavior of the Zr and B-containing hybrid polymeric precursor was studied. The densification behaviour was investigated through the analysis of the microstructures of CBCFs-SiC-ZrB₂ (denote as CSZ) composites with different density. The mechanical properties, thermo properties and oxidation behavior of CSZ composites were studied. The results show that the incorporation of ZrB₂ ceramic coating does not change the anisotropic properties of CBCF composites. The CSZ composites with a density of 0.77 g/cm³ with continuous ZrB₂ ceramic coated layer on the surface of the carbon fibers which exhibit better mechanical properties and antioxidant properties. The composites show the remarkable thermo properties which are better for thermal insulation applications.

Corresponding author: Tel/fax: +86 451 86403016. E-mail: hongcq@hit.edu.cn (C. Hong)

1. Introduction

Low-density C/C composites, i.e., carbon-bonded carbon fiber composites (CBCFs) have been used extensively for thermal insulation applications owing to its light weight, low thermal conductivity, and high temperature capability^[1, 2]. Often they consist of chopped carbon fibres network bonded together at the intersections of the fibres by discrete regions of vitreous carbon, and the open porosities range from 70 to 90%^[3, 4]. A consequence of the vacuum or pressured molding process^[5, 6] used in composite production is that the discontinuous carbon fibers are orientated into layers to form a 2D planar random structure. The high porosity content and fiber orientation result in a low thermal conductivity perpendicular to the fiber layer arrays (z-direction), hence their use as high temperature insulation and thermal protection materials matrix. Up to now, the microstructures^[7], mechanical properties^[8], and thermal properties^[9, 10] of CBCFs have been reported elsewhere. However, there are mainly two technical problems to be solved for the application of CBCFs: (i) the mechanical strength must be improved to resist the gas particle erosion at chemical and thermal environment; (ii) the oxidation-resistance should be enhanced to overcome the weakness of lightweight carbon-based composites.

The carbon surface coated with inorganic materials attracts great interest that can improve the properties of carbon^[11- 13]. The introduction of ultra-high temperature ceramics (UHTCs) (i.e., ZrB₂, ZrC, HfC or SiC) into these low-density C/C composites has been proved to improve the high temperature performance of C/C composites. Different processing methods including slurry infiltration^[14, 15], precursor

infiltration and pyrolysis (PIP)^[16-17], reactive melt infiltration^[18-20], chemical vapor decomposition^[21], thermal spray technology and combination of them^[22], have been successfully used to prepare C/C-UHTCs composites. Meanwhile, the oxidation and ablation behavior of ZrC/C^[23], C/C-ZrC^[24], and C/C-ZrB₂ composites^[25] evaluated by oxyacetylene torch were improved than that of pristine C/C composites when more ingredients of UHTCs were added.

In the last few years, there is less information available in literature about CBCFs modified by UHTCs. There have been few works making a direct comparison between CBCFs and CBCFs-UHTCs composites, it is difficult to assess whether or not the UHTCs additive is beneficial to the improvement of mechanical and thermal properties of CBCFs. In this study, the low density and porous CBCFs containing chopped carbon fibers were prepared based on our previous work^[6] and the SiC-modified CBCFs were prepared by Zhang^[26]. To prepare the ZrB₂ and SiC-modified CBCFs composites, PIP method was adopted using novel B and Zr polymeric precursor in our research. The microstructure, mechanical, and thermal properties were investigated in detail.

2. Experimental

C_f (Jilin Jiyan High-tech Fibers Co., Ltd. Jilin, China), SiC (1μm, purity>99.5%, Weifang Kaihua Micropowder Co., Ltd., Weifang, China) and P_f (PF4090, fineness>95%/200 mesh, Holy spring chemical co., Ltd., Juxian, China) were used as raw materials for SiC-modified CBCFs. SiC-modified CBCFs were prepared by an effective dispersion and flocculent approach using 0.6wt.% polyethylene imine as a

dispersant and 0.8wt.% polyacrylamide as a flocculating agent. The preparation details have been reported elsewhere ^[26]. The cylindrical SiC-modified CBCFs with a size of $\Phi 30 \times 20$ mm and density of 0.26 g/cm^3 (denote as CS-0.26) were employed as preforms for ZrB_2 -modified CS composites (denote as CSZ).

The component content of Zr-containing precursors and B-containing precursors (Institute of Process Engineering, Chinese Academy of Science, China) were listed in Table 1. The Zr-containing precursor was $[(\text{C}_4\text{H}_8\text{O})\text{Zr}(\text{acac})_2]_n$ with molecular weight about 64870 and a softening point of 170°C . The B-containing material was 2, 4, 6-tri-methylamino borazine with the chemical formula $(\text{NHCH}_3)_3\text{B}_3\text{N}_3\text{H}_3$ and molecular weight ~ 600 ^[27]. The 66.7wt% polymeric precursor solution was prepared by dissolving Zr-containing polymeric precursor and B-containing precursor (with a B/Zr molar ratio of 2) into dimethylbenzene.

The CS-0.26 was impregnated into polymeric precursor using a vacuum infiltration device, drying at 80°C in a drying oven in Ar atmosphere. The pyrolysis was performed at a heating rate of $2^\circ\text{C}/\text{min}$ to the desired temperature of 1500°C and then held for 2h under flowing Ar atmosphere. The mass of ZrB_2 in the CSZ composites was calculated by weighing the CS before the procedure of impregnation and after heat treatment. The content of ZrB_2 in the CSZ was calculated by the ratio of the mass of ceramic and the CS. The obtained different contents of ceramic were attributed to the impregnated times of the CS. The CS were densified to the density of 0.40, 0.61 and 0.77 g/cm^3 by PIP repeated, and the obtained CSZ composites were denoted as CSZ-0.40, CSZ-0.61 and CSZ-0.77, respectively.

The thermal analysis technique which combined with thermogravimetric analysis (TGA) and differential scanning calorimetry (DSC) was used to analyze the thermal behavior of the hybrid precursors during the pyrolysis process. The test condition was like this: the reference compound Al_2O_3 with flowing Ar, the scanning temperature range from 25°C to 1600 °C, the heating rate of 10 °C/min. The TG-DSC technique also employed to analyze the antioxidant properties of CSZ and CS in flowing air.

The oxidation behavior of the CS and CSZ-0.77 samples with the size of 10×10×10 mm³ were machined from bigger blocks was evaluated by the isothermal oxidation test, which was carried out in static air in an electrical furnace at 800°C. During the isothermal oxidation test, the samples will be taken out of the electronic furnace for the designated time, which were quickly cooled to room temperature and weighed by an electronic balance with a sensitivity of ±0.1mg. The weight change percentages were calculated and reported as a function of oxidation time according to the formula: $\Delta W\% = (m_0 - m_t) / m_0 \times 100\%$, where m_0 and m_t are the weight of the specimens before oxidation and after oxidation, respectively.

The phase composition of the hybrid precursor at different pyrolysis temperature and the CBCFs, CS and CSZ with different density were investigated by a Rigaku D/max-rb X-ray diffraction(XRD). The morphology and of the composites was investigated by a Holland FEI Sirion scanning electron microscopy (SEM) equipped with energy dispersive spectroscopy (EDS). Compression testing tests were performed on a Suns Co. CMT-5304 electronic universal testing machine to determine the mechanical property of the composites. Specimens were tested parallel to the x/y

and z axes with the compressive property anisotropy ratio being defined as the ratio of mechanical property values in the x/y and z planes. The samples were machined from bigger blocks and the effective size of the samples was $10 \times 10 \times 12 \text{ mm}^3$ and at a crosshead speed of 2 mm min^{-1} .

The composites were cut into disk-shape with diameters of 12.7 mm and thicknesses of approximately 1.6 mm, and the thermal diffusivities in the x/y and z direction of the samples were determined by laser flash method using a Netzsch LFA 427 apparatus in Ar. The CTE measurements were carried out on a Netzsch DIL 402 dilatometer with a heating rate of $2^\circ\text{C}/\text{min}$.

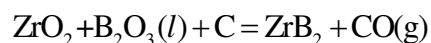
3. Results and discussion

3.1. Pyrolysis behavior of the hybrid precursor

The TGA–DSC technique is performed to understand the thermal behavior of the hybrid precursors during the pyrolysis process, as shown in Fig. 1. The TGA shows that the thermal degradation process can be divided into three temperature ranges. The first weight loss is 8.59 wt% up to 300°C . A broaden endothermic peak near 150°C (shown in “A” peak of the DSC profile) was likely to be due to the loss of low molar mass oligomers and water (the hybrid precursors are very sensitive to moisture and oxygen). The second weight loss is 33.24wt% between 300 and 600°C associated with an exotherm peak near 430°C (“B” peak) due to the broken of C and N containing gas (i.e., CH_4 , CO , CO_2) from hybrid precursors (the gas species result from broken organic bonds and recombination processes)^[28]. Whereas the third one is 26.00 wt% weight loss from 1100 to 1500°C . A remarkable endothermic peak near 1440°C (“D”

peak)) ascribe to C and N containing gas further release and the important ceramic process^[27]. In addition, very little weight loss is observed between 600 and 1100°C about 3.9% weight loss. The exothermic reaction occurs at 680 °C (“C” peak). The result shows in a total ceramic yield of 33.45% at 1500 °C.

The XRD patterns of the samples are obtained to investigate the crystallization evolution of the B and Zr hybrid precursors. Only a very broad peak is observed at 600°C (Fig. 2 (a)), which indicates that the product almost does not crystallize at these temperatures. The t-ZrO₂ is observed when the temperature reached 900°C (Fig. 2 (b)). A little amount of m-ZrO₂ is detected in Fig. 2 (c) at 1200 °C. Even the hybrid precursors are heated to 1400 °C (Fig. 2(d)), the peaks of m-ZrO₂ are noticeable, and initial formation of ZrB₂ phase is observed. A great change is present when heating to 1500°C (Fig. 2(e)). The sharpening of the characteristic peaks of ZrB₂ is noticeable, where no any other phase is observed. The following reactions occurred during pyrolysis process:



3.2. Microstructure and densification behavior of CSZ composites

The bulk density, open porosity, ZrB₂ content of porous CSZ composites are listed in Table 2, which indicate that the density increases from 0.26 to 0.77 g/cm³ and the open porosity decreases from 84.71 to 43.81% when the ZrB₂ content increases from 0 to 52.31wt.%.

Fig. 3 shows XRD patterns of the CBCFs, CS and CSZ with different density. It reveals that the CBCFs are mainly composed of carbon and the CS are carbon and

SiC. With the increasing density of prepared CSZ, the peak intensities of carbon and SiC become weaker, while the relative peak intensities of ZrB_2 become higher. A little amount of SiC was observed in C-0.61 samples, while pure ZrB_2 phase was seen in CSZ-0.77 which was attributed to the complete layering on the surface of carbon fibers.

The microstructural morphology of CSZ composites is shown in Fig.4, illustrating the typical microstructure of CSZ composites with different ZrB_2 content. Fig. 4(a), (c) and (e) indicate that C-0.40 sample has many open pores, however, the pores contents are remarkably decreased when the ZrB_2 content increased from 33.33 to 65.45wt.%. The microstructure of ceramic layer on the carbon fiber surface with high magnification is shown in Fig. 4(b), (d) and (f), revealing the ZrB_2 ceramics are increased and densified with the increasing times of impregnation-pyrolysis cycles. More and more B and Zr polymeric precursor will transform to ZrB_2 ceramics and coated onto carbon fiber surface with the increasing of density. In the first stage, since the ceramic volumetric shrinkage occurs in pyrolysis process, the carbon fibers are coated by uncontinuous ceramics, as shown in Fig. 4(b). The second stage, the new forming ceramic layer continue to infiltrate the ceramic fissures or pores and further overlayer the carbon fibers (Fig. 4(d)). More ZrB_2 ceramics impregnated into the pores of CS and coated carbon fibers with the further increasing of ZrB_2 content (Fig. 4(f)). Finally the carbon fibers are surrounded by a continuous ZrB_2 ceramic matrix and no bare carbon fibers are found.

3.3. Mechanical property of CS and CSZ composites

Fig. 5 shows the mechanical properties of the CS modified by ZrB_2 . Compared to the CS, the compressive strength and modulus of the CS modified by ZrB_2 have been improved. The compressive strength (Fig. 5(a)) and modulus (Fig. 5(b)) of the as-received composites increases with the increasing of ZrB_2 content. It indicates that mechanical properties of CSZ composites in x/y direction are superior to the z direction compared to equivalent-density specimens which is in agreement with previous work of CBCFs^[6]. The following affecting factors are attributed to this variation (i) the introduction of ZrB_2 ceramic increases the mechanical strength; (ii) The carbon fibers are oriented preferentially and arranged randomly in x/y direction, as a result of the manufacturing process, making it a transversely isotropic material of CSZ composites.

Fig. 6 illustrates typical compressive stress-strain curves for CSZ-0.77 composites in x/y direction and z direction. The compressive strength in x/y direction is significantly stronger and stiffer with increasing ZrB_2 content, which is indicated by an increase in the slope for initial linear region and the maximum strength in Fig. 6(a). The curves variation in x/y direction showed a linear elastic deformation up to its failure stress, which is in agreement with CBCFs coating by SiC^[8]. The deformation mainly experiences three stages in z direction, namely AB, BC, and CD, as show in CSZ-0.77 sample (Fig. 6(b)). The AB region is linear and elastic, and the other regions BC and CD are inelastic. Complete disintegration of the specimen was observed upon reaching maximum stress with a large proportion of “dust debris” for x/y direction and “dust powders” for z direction remaining at the end of the test (not

shown here). The elastic deformation of this stage is believed to be formed through elastic bending and rotation of reinforcing fibers. In the following non-elastic region until the maximum stress, the slope which indicates the modulus for x/y direction is extremely larger than that of z direction. This can be explained by the much denser structure in x/y plane than z direction, and consequently less elastic deform at a given applied stress which determines the modulus.

3.4. The thermal performance of CSZ-0.77 composites

The thermal conductivity of the CS and CSZ-0.77 composites are performed from 25.5 °C to 1001.7 °C, as show in Table 3. The thermal conductivity for x/y direction and z direction are higher than CS. The thermal conductivity of CSZ increases at a slightly greater rate from 25.5 to 251.5 °C (0.524 -0.829 W/mK for x/y direction and 0.237-0.413W/mK for z direction), while from 251.5 to 1001.7°C, all of the samples exhibited similar thermal conductivity (0.829-0.883 W/mK for x/y direction and 0.413-0.473 W/mK for z direction). That is not only solid thermal conductivity, but also radiation and gas thermal conductivity contributes to the overall thermal conductivity at higher temperature^[6]. As can be seen, the thermal conductivity for x/y direction is even higher than the thermal conductivity for z direction. The thermal conductivity for CSZ-0.77composites is determined by ceramic matrix, carbon fibers and pores. The ceramic matrix must transmit the heat to the fibers and the fibers as “wick” take the heat away from a source. The orientation of the most fibers and the heat source are in the same plane for x/y direction, which contributes to heat conduction. While most fibers are perpendicular to the heat source for z direction, the

heat flow will cause thermal diffusion and insulate the flow of heat through z direction. Moreover the porosities in x/y direction are less than in z direction which is beneficial to heat conduction.

The CTE of CSZ-0.77 sample is shown in Fig. 6. The CTE at z direction and x/y direction is from 0.14×10^{-6} to $1.19 \times 10^{-6}/K$ and from 0.17×10^{-6} to $0.69 \times 10^{-6}/K$, respectively, from 67 to 400°C. The isotropy thermal expansion in the CBCFs directly results from the isotropy of the CTE of the fibers, the porosity and the major component of CBCFs ^[29]. Furthermore, for the ZrB₂ reinforced CS, the addition of ceramic components also will contribute to the CTE of CSZ composites. The ceramic layer is coated onto the fibers, as seen in Fig. 4, so the fiber arrangement will affect the CET of CSZ composites. In this case, the fiber coated by ZrB₂ will show a greater expansion in the x/y direction as opposed to that in the z direction. Considering the microstructural anisotropy, the fibers lie preferentially in the x/y direction but are random in direction within those planes ^[30]. Along the x/y direction, the fibers are random and therefore the contribution of the higher radial expansion is limited. On the other hand the majority of fibers lie perpendicular to the z direction and so the contribution of the large radial expansion to the overall expansion along this direction is proportionately high. Therefore, the z direction radial orientation of the ZrB₂ around the fibers would account for the CTE of CSZ composites being greater in the z direction compared to that in the x/y direction. On the other hand, CSZ composites contain various micropores, so that they have a different effect on the CTE for the samples at x/y direction between 67 and 86°C and z direction between 67 and 127°C.

When the CSZ composites is heated in a condition of lower temperature, the volatilization of the absorbed water in them make the pores shrink, and the more porosity allows the composites to absorb more water, which results in more shrinkage with the temperature as shown in Fig. 7. However they do not present negative expansion behaviors in the range 0-100 °C, which is different from common C/C composites^[31], due to the ZrB₂ layers intensive restrict shrinkage. In addition, the result shows an interesting phenomenon, the anisotropic structures do not result in an anisotropic thermal expansion between 50 and 60°C.

3.5 Oxidation behavior of CS and CSZ-0.77 composites

The GA–DSC technique in flowing air is used to analyze the oxidation behavior of the CSZ-0.77 composites, whilst CS composites without ZrB₂ coating are used for sake of comparison. Fig. 8 shows the TG-DSC thermogram of the CS samples below 1500°C. As shown in this figure, there is an endothermic peak at 98°C (shown in “A” peak of the DSC profile) due to the evaporation of water absorbed in composites, corresponding to about 4.65% weight loss. It can be attributed to the moisture evaporation. Carbon fibers and pyrolytic carbon are oxidized between about 517 and 736°C, and the weight loss is about 61.21%. A corresponding exothermic peak is observed near 648 °C (“B” peak), which is ascribed to carbon oxidation to form CO and CO₂. Above 1100°C, SiC reacts with O₂^[32], corresponding to about 3.52% weight gain.

Fig. 9 describes the TGA–DSC profile of ZrB₂ coated CS composites. TG analysis shows that a weight loss about 1.6% occurs at about 146°C due to the

evaporation of water absorbed in composites, which results in an apparent endothermic peak (“A” peak) in the DSC curve. The weight of the samples decreases quickly between 742 and 1000°C. The weight loss is about 30.07%. The corresponding exothermic peaks near 818 (“B” peak) and 888 °C (“C” peak) are observed in the DSC curve. The “B” peak can be ascribed to apart of C (carbon fibers and pyrolytic carbon) oxidation to form CO and CO₂. The “C” peak can be ascribed to ZrB₂ oxidation into ZrO₂ and B₂O₃^[33]. The weight lose is about 8.14% due to the weight gain by ZrB₂ oxidation dose not makes up with the weight lose by C oxidation. Thus, many CO and CO₂ gases escape, and B₂O₃ evaporation leads to the weight of sample decreases from 888 to 1000°C. As the carbon decrease, CO and CO₂ gases escapes slowly down, which make the weight gain about 3.01% due to the oxidation of ZrB₂ and SiC between 1000 and 1263°C. After 1263°C, the weight of B₂O₃, CO and CO₂ evaporation and more than the weight gain of oxidation of ZrB₂ and SiC which result in the weight lose.

Compared with the oxidation behavior of CS, a remarkable improvement in the oxidation resistance was observed. The beginning oxidation temperature of ZrB₂ coated is raised from 517°C to 742°C. The largest weight loss of composites without ZrB₂ coating is near 736°C, whilst the ZrB₂ coated ones are near 1025°C. Therefore, the coating of infusible compound ZrB₂ on the CS can effectively improve the oxidation resistance.

In order to further investigate the oxidation behavior of the CSZ-0.77 at fixed temperature, the isothermal oxidation tests were performed at 800°C in air. Fig. 10

shows the backscattering images (BSE) image and EDS analysis of the cross-section of the CS and CSZ-0.77 after isothermal oxidation at 800 °C for 30 and 60min, respectively. Fig. 4(a) indicates that there is no appearance of carbon fibers in CS due to the complete oxidation of carbon fiber. According to the EDS analysis (Fig. 10(e)), it conforms that the oxidized CS is only composed of SiO₂. The high magnification micrograph (Fig. 10(b)) shows that SiO₂ is tended to be granular and aggregated along the direction of carbon fiber. However, the residual carbon fibers after oxidation were found in Fig. 10(c), which indicates that the oxidation resistance has been improved by introducing ZrB₂ into CBCFs. From the Fig. 10(d), the residual carbon fiber surface was covered by oxide layer and the oxide layer is mainly composed of ZrO₂ and with a little amount of SiO₂ and B₂O₃ by EDS analysis (Fig. 10(f)). The ZrO₂-SiO₂-B₂O₃ layer on the carbon surface will prevent the carbon matrix directly from oxidation, which can improve the oxidation resistance of CBCFs significantly.

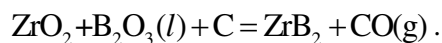
The weight change of CS and CSZ-0.77 after isothermal oxidation tests are shown in Fig. 11. The results show that the weight loss of the CS and CSZ-0.77 is 62.4% and 24.1% after isothermal oxidation at 800°C for 60min, while the carbon content is about 77.19% and 39.01% in CS and CSZ-0.77, respectively. According to the Fig. 11 (a) and (b), it is indicated that there is 14.79% weight gain in CS due to the weight gain reaction of SiC oxidation. However, the 14.91% weight gain in CSZ-0.77 is due to the existence of residual carbon after oxidation and the oxidation gain of ZrB₂ and SiC. The weight loss of CSZ-0.77 presents significant reduction before 40 min because of the oxidation of bare carbon on the surface of samples, while the

ZrO₂-SiO₂-B₂O₃ layer was formed on the surface of carbon fibers after 40min. It can thus be concluded that the oxidation ability of the composites can be obviously improved by the incorporation of ZrB₂.

4. Conclusions

The CSZ composites were prepared by PIP using B and Zr polymeric precursor. The Microstructure and properties of lightweight CSZ composites was investigated in this paper. The results suggest that the CSZ composites are important considerations for potential use in thermal protection system applications.

(1) The ZrB₂ ceramic forms during pyrolysis at 1500°C through the reaction:



(2) The CBCFs were fully coated by ZrB₂ ceramics and there is no bare fiber found in composites when the ceramic content is 52.31%. The density increases from 0.26 to 0.77 g/cm³ and the open porosity decreases from 84.71 to 43.81%.

(3) The properties of lightweight CSZ composites show anisotropic between *x/y* direction and *z* direction due to the anisotropic structures. The compressive strength ranged from 1.36 to 2.83 MPa and from 0.61 to 1.63 MPa for *x/y* direction and *z* direction, respectively, with different densities. The thermal conductivity for the composites of CSZ-0.77 sample is 0.524-0.883 and 0.237-0.473 Wm⁻¹K⁻¹ for the directions perpendicular and parallel to the pressure, respectively, at 25.5-1001.7°C. The CTE at *z* direction and *x/y* direction is from 0.14×10⁻⁶/K to 1.19×10⁻⁶/K and from 0.17×10⁻⁶/K to 0.69×10⁻⁶/K, respectively, from 67 to 400°C.

(4) The TGA–DSC results showed that the beginning oxidation temperature of ZrB₂ coated is raised from 517°C to 742°C and the largest weight loss of composites without ZrB₂ coating is near 736°C, whilst the ZrB₂ coated ones are near 1025°C. The isothermal oxidation tests showed that the complete oxidation of CS is about at 30min, while the CSZ-0.77 is not complete oxidation even at 60min at 800°C. The coating of infusible compound ZrB₂ on the CS can improve the oxidation resistance.

Acknowledgments

This research was financially supported by the National Natural Science Foundation of China (No.51272056, 11121061 and 91216301).

References

- [1] T. Moskalwwicz, F. Smeacetto, M. Salvo, A. R. Boccaccini and A. Czyrska-Filemonowicz, *J. Microsc.*, 2010, 237(3), 288–291.
- [2] I. J. Davies and R. D. Rawlings, *Compos. Sci. Technol.*, 1999, 59, 97–104.
- [3] A. S. Ahmed, R. D. Rawlings, S. D. Ellacott and A. R. Boccaccini, *J. Eur. Ceram. Soc.*, 2011, 31, 189–197.
- [4] R. I. Baxter, R. D. Rawlings, N. Iwashita and Y. Sawada, *Carbon*, 2000, 38(3), 441–449.
- [5] I. J. Davies and R. D. Rawlings, *J. Mater. Sci.*, 1994, 29, 338–344.
- [6] C. Liu, J. C. Han, X. H. Zhang and S. Y. Du, *Carbon*, 2013, 59, 547–554.
- [7] G. C. Wei and J. M. Robbins, *Am. Ceram. Bull.*, 1985, 64, 691–699.
- [8] A. S. Ahmed, Z. Chlup, I. Dlouhy, R. D. Rawlings and A. R. Boccaccini, *Int. J. Appl. Ceram. Technol.*, 2012, 9, 401–412.
- [9] F. Smeacetto, M. Ferraris, M. Salvo, S. D. Ellacott, A. Ahmed, R. D. Rawlings,

- and A. R. Boccaccini, *Ceram. Int.*, 2008, 34, 1297–1301.
- [10] A. S. Ahmed, R. D. Rawlings, S. D. Ellacott and A. R. Adv. Appl. Ceram., 2012, 0(0), 1–9.
- [11] L. Zhang, D. S. Zhang, J. P. Zhang, S. X. Cai, H. R. Li, R. H. Gao and L. Y. Shi, *Nanoscale*, 2013, 5, 9821–9829.
- [12] D. S. Zhang, L. Zhang, L. Y. Shi, C. Fang, H. R. Li, R. H. Gao, L. Huang and J. P. Zhang, *Nanoscale*, 2013, 5, 1127–1136.
- [13] C. Fang, D. S. Zhang, S. X. Cai, L. Zhang, L. Huang, H. R. Li, P. P. Maitarad, L. Y. Shi, R. H. Gao and J. P. Zhang, *Nanoscale*, 2013, 5, 9199–9207.
- [14] H. J. Li, D. J. Yao, Q. G. Fu, L. Liu, Y. L. Zhang, X. Y. Yao, Y. J. Wang and H. L. Li, *Carbon*, 2013, 52, 418–426.
- [15] C. X. Liu, L. X. Cao, J. X. Chen, L. A. Xue, X. Tang and Q. Z. Huang, *Carbon*, 2013, 65, 196–205.
- [16] H. T. Wu, X. Wei, S. Q. Yu and W. G. Zhang, *J. Inorg. Mater.*, 2011, 26(8), 852–856.
- [17] K. Z. Li, X. Jing, Q. G. Fu, H. J. Li, L. J. Guo, *Carbon*, 2013, 57, 161–168.
- [18] L. H. Zou, N. Wali, J. M. Yang and N. P. Bansal, *J. Eur. Ceram. Soc.*, 2010, 30(6), 1527–1535.
- [19] Z. Q. Li, H. J. Li, S. Y. Zhang, J. Wang, W. Li and F. J. Sun, *Corros. Sci.*, 2012, 58, 12–9.
- [20] Y. G. Wang, X. J. Zhu, L. T. Zhang and L. F. Cheng, *Ceram. Int.*, 2011, 37(4), 1277–83.
- [21] Y. B. Fei, J. H. Lu, H. J. Li, L. J. Guo and Z. S. Chen, *Vacuum* 2013, doi:10.1016/j.vacuum.2013.10.018.
- [22] C. Hu, Y. R. Niu, H. Li, M. S. Ren, X. B. Zheng and J. L. Sun, *J. Therm. Spray.*

- Techn., 2012;21(1):16–22.
- [23] D. Zhao, C. G. Zhang, H. F. Hu and Y. D. Zhang, *Compos. Sci. Technol.*, 2011, 71(11), 1392–1396.
- [24] W. Sun, X. Xiong, B. Y. Huang, G. D. Li, H. B. Zhang, Z. K. Chen and X. L. Zheng, *Carbon*, 2009, 47, 3365–3380.
- [25] H. J. Li, X. Y. Yao, Y. L. Zhang, K. Z. Li, L. J. Guo and L. Liu, *Corros. Sci.*, 2013, 74, 265–270.
- [26] X. H. Zhang, B. S. Xu, C. Q. Hong, J.C. Han, F. X. Qin, W. B. Han, H. M. Cheng, C. Liu and R. J. He, *RSC Adv.*, 2014, 4, 6591–6596.
- [27] C. M. Xie, M. W. Chen, X. Wei, M. Ge and W. G. Zhang, *J. Am. Ceram. Soc.*, 2012, 95(3), 866–869.
- [28] E. Bouillon, F. Langlais, R. Pailler, R. Naslain, F. Cruege and P. V. Huong, *J. Mater. Sci.*, 1991, 26, 1333–1345.
- [29] R. I. Baxter, R. D. Rawlings, N. Iwashita and Y. Sawada, *Carbon*, 2000, 38, 441–449.
- [30] I. J. Davies and R. D. Rawlings, *J. Mater. Sci.*, 1994, 29(2), 338–344.
- [31] R. I. Baxter, R. D. Rawlings, N. Iwashita and Y. Sawada, *Carbon*, 2000, 38, 441–449.
- [32] W. M. Guo and G. J. Zhang, *J. Eur. Ceram. Soc.*, 2010, 30, 2387–2395.
- [33] P. Hu, G. L. Wang and Z. Wang, *Corros. Sci.*, 2009, 51, 2724–2732.

Tables

Table 1 Component contents (wt%) of the Zr-containing and B-containing precursors ^[27].

Component	Zr (%)	O (%)	N (%)	C (%)	B (%)	H (%)
Zr-containing precursor	29.8	26.4	–	37.9	–	5.88
B-containing precursor	–	–	34.41	29.89	27.25	8.34

Table 2 Properties of porous CS and CSZ composites.

Specimen number	Density (g/cm ³)	Content of ZrB ₂ (wt. %)	Porosity (%)
CS-0.26	0.26	0	84.71
CSZ-0.40	0.40	12.32	72.53
CSZ-0.61	0.61	43.56	55.52
CSZ-0.77	0.77	52.31	43.81

Table 3 Thermophysical properties of CS and CSZ-0.77 composites

Temperature (°C)	x/y direction		z direction	
	$\lambda_{xy(cs)}$ (W/mK)	$\lambda_{xy(cs-0.77)}$ (W/mK)	$\lambda_{z(cs)}$ (W/mK)	$\lambda_{z(cs-0.77)}$ (W/mK)
25.5	0.296±0.02	0.524±0.02	0.110±0.01	0.237±0.03
251.5	0.211±0.01	0.829±0.04	0.112±0.01	0.413±0.05
501.5	0.219	0.841±0.09	0.131±0.02	0.457±0.03
751.7	0.252±0.03	0.870±0.05	0.148±0.02	0.471±0.14
1001.7	0.298±0.06	0.883±0.17	0.211±0.07	0.473±0.42

Figures

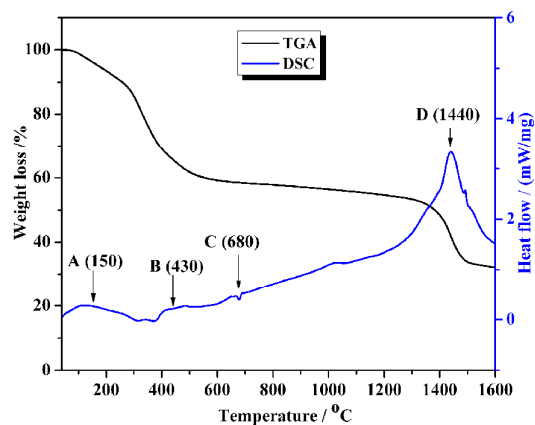


Fig. 1. TGA and DSC profile of B and Zr hybrid precursor.

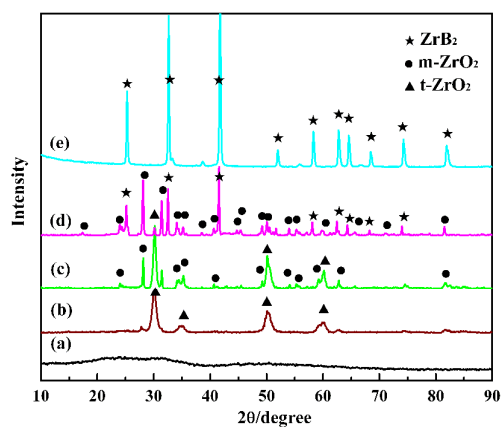


Fig. 2. XRD patterns of the B and Zr hybrid precursors heat-treated at various temperatures: (a)600°C; (b)900°C; (c)1200°C;(d)1400°C and (e)1500°C.

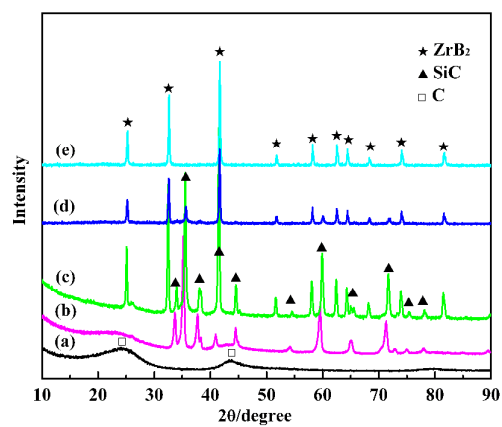


Fig. 3. XRD patterns (a) CBCFs; (b) CS; (c) CSZ-0.40; (d) CSZ-0.61; (e) CSZ-0.77.

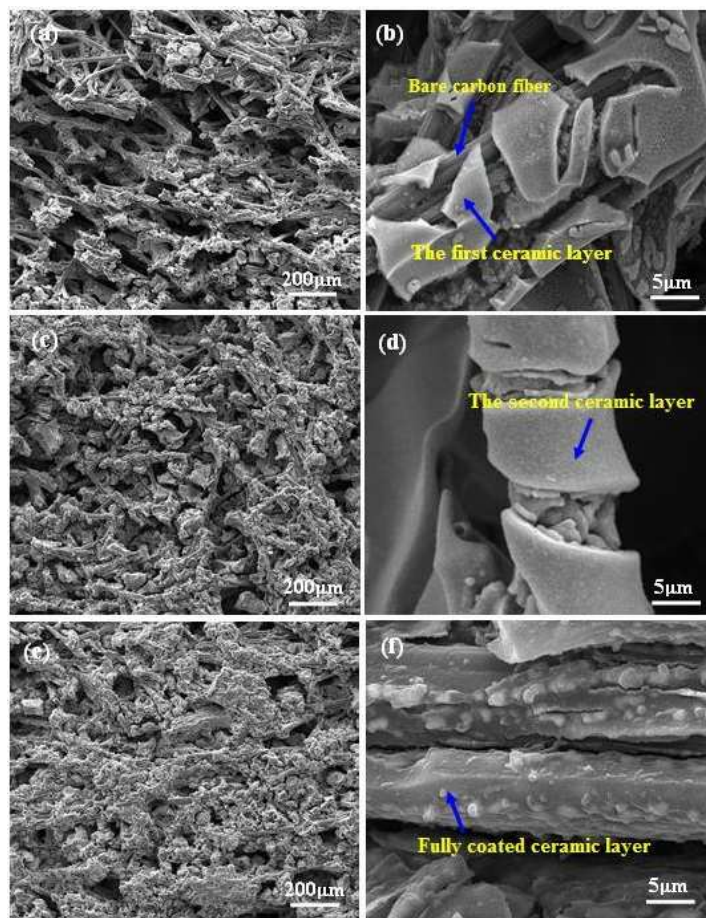


Fig. 4. Cross-section microstructure of CSZ composites (a) CSZ-0.40; (c) CSZ-0.61; (e) CSZ-0.77; (b), (d) and (f) high magnification in (a), (c) and (e), respectively.

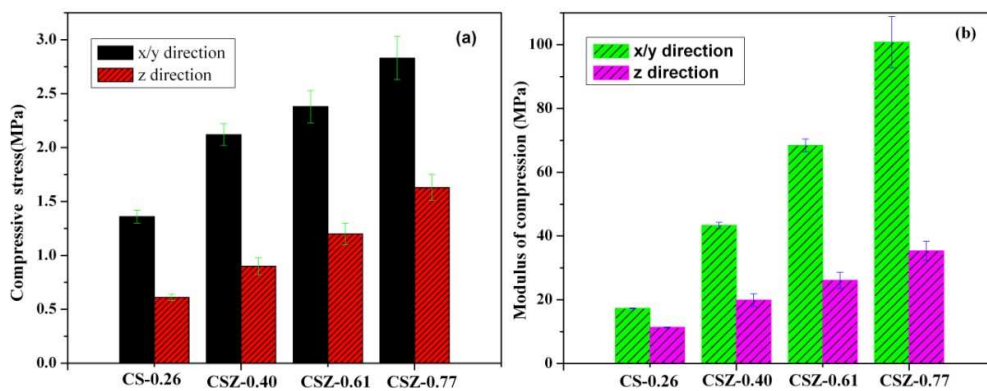


Fig. 5. Mechanical properties of CSZ and CS-0.26. (a) Compressive strength; (b) Modulus of compression.

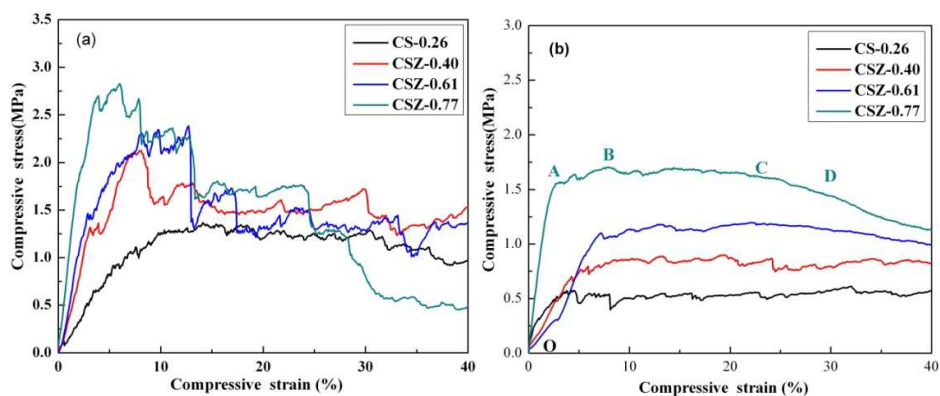


Fig. 6. Typical compressive stress/strain curves for ZrB_2 -modified CS (a) x/y direction; (b) z direction.

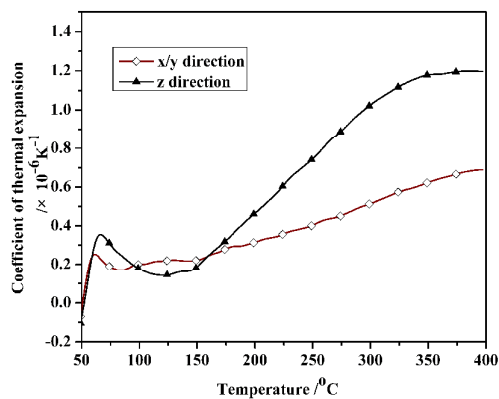


Fig. 7. The CTE of CSZ-0.77 composites.

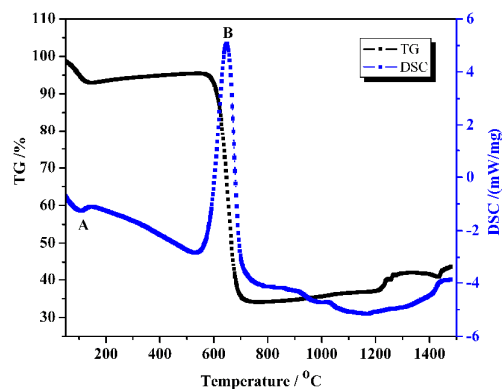


Fig. 8. TGA and DSC profile of the CS composites

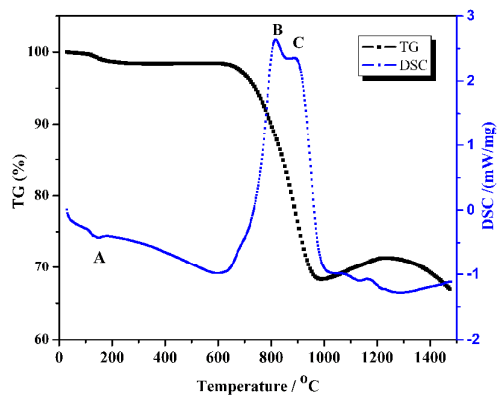


Fig. 9. TGA and DSC profile of C-0.77

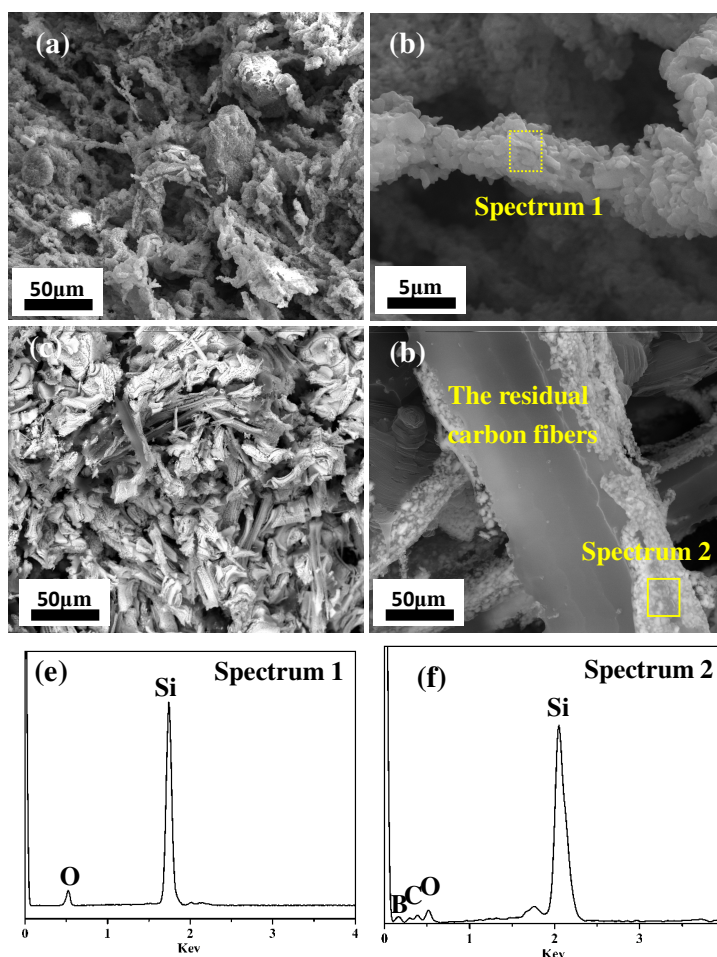


Fig. 10. Cross-section backscattering images and EDS analysis of the CS and CSZ-0.77 after oxidation at 800 °C for 60 min.(a) and (b) low magnification and high

magnification of CS; (c) and (d) low magnification and high magnification of CSZ-0.77; (e) and (f) EDS analysis.

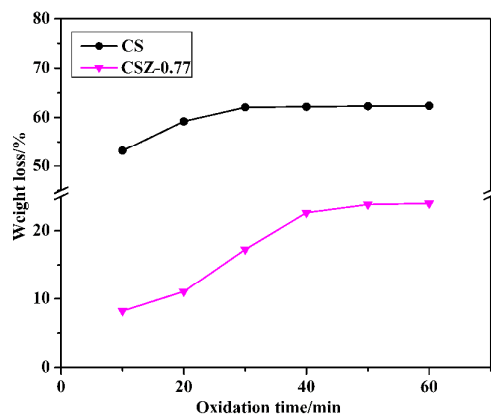


Fig. 11. Isothermal oxidation curve of CS and CSZ-0.77 at 800°C in air.